Nonlinear Dyn (2021) 104:4523–4541
https://doi.org/10.1007/s11071-021-06476-2

ORIGINAL PAPER

A fractional-order multistable locally active memristor and its chaotic system with transient transition, state jump

Wenli Xie · Chunhua Wang · Hairong Lin

Received: 17 December 2020 / Accepted: 15 April 2021 / Published online: 2 May 2021

Abstract Fractional calculus is closer to reality and has the same memory characteristics as memristor. Therefore, a fractional-order multistable locally active memristor is proposed for the first time in this paper, which has infinitely many coexisting pinched hysteresis loops under different initial states and wide locally active regions. Through the theoretical and numerical analysis, it is found that the fractional-order memristor has stronger locally active and memory characteristics and wider nonvolatile ranges than the integer-order memristor. Furthermore, this fractional-order memristor is applied in a chaotic system. It is found that oscillations occur only within the locally active regions. This chaotic system not only has complex and rich nonlinear dynamics such as infinitely many discrete equilibrium points, multistability and anti-monotonicity but also produces two new phenomena that have not been found in other chaotic systems. The first one is transient transition: the behavior of local chaos and local period transition alternately occurring. The second is state jump: the behavior of local period-4 oscillation or local chaotic oscillation jumping to local period-2 oscillation. Finally, the circuit simulation of the fractional-order multistable locally active memristive chaotic system using PSIM is carried out to verify the validity of the numerical simulation results.

Keywords Locally active memristor · Multistable · Fractional order · Transient transition · State jump · Anti-monotonicity

W. Xie · C. Wang (✉)· H. Lin
College of Computer Science and Electronic Engineering
Hunan University, Changsha 410082, China W. Xie
e-mail: wlxie123456@163.com

C. Wang
e-mail: wch1227164@hnu.edu.cn

H. Lin
e-mail: haironglin66@126.com

1 Introduction

Fractional calculus is an extension of integral calculus. Because the objects are usually fractional order, in real life [1], it is more accurate to describe objects using fractional order than integer order. In addition, fractional calculus has the memory characteristic with respect to time. Memristor is the fourth fundamental circuit element which is widely used in chaotic neural networks [1–8], circuit design [9–12], secure communications [13–17], bio-simulation circuit [18] and logic circuit [19]. Memristor has the same memory characteristic as fractional calculus, so memristor can be extended to fractional order. Coopmans et al. proposed the concept of fractional-order memristive systems and investigated the mathematical relationship between the dynamics of memristive systems and the fractional calculus [20]. Petras proposed a fractional-order flux-controlled memristor for the first time and applied it in Chua's circuit. By fractional-order differential, they got a chaotic system in which total order less than three [21]. Cafagna and Grassi proposed the sim-

plest fractional-order memristive chaotic system and proved the existence of chaotic attractors by numerical simulation. They also used 0-1 test to further confirm the existence of chaos [22]. A fractional-order quartic polynomial memristive Chua's circuit can generate a four-scroll attractor and the effect of initial value and fractional order on dynamics was studied [23]. Si et al. proposed a fractional-order charge-controlled memristor and found triple-loop I–V curves for the first time whose area decreased with the decrease of fractional order [24]. Yang and Xu proposed a fractional-order flux-controlled memristor and gave the computational formulas of areas of pinched hysteresis loops. Besides, the effect of fractional order on the memristor was studied [25]. Yu and Wang investigated the fractional-order HPTiO-2 memristor model and discussed the voltage–ampere characteristics of the circuit in which the memristor was in series with capacitance or inductance [26]. In Ref. [27], the fractional-order Chua's circuit model with a fractional-order memristor was proposed and the intermittent chaos caused by bifurcation was studied.

The locally active was defined by Chua [28], it is the origin of complexity [29], because it provided an effective method to study complex nonlinear dynamics. Locally active devices are necessary for oscillating systems [30]. Oscillations occur only in locally active regions. Refs. [31,32] stated that the nonlinear dynamics of locally active memristors are richer with the increase of the number of stable equilibrium points. However, a lot of published locally active memristors have only one to three stable pinched hysteresis loops and limited locally active regions. For example, Chua proposed a corsage memristor with one pinched hysteresis loop and limited locally active ranges [33]. Mannan et al. analyzed Chua's corsage memristor from the bifurcation chart and complex frequency domain. The oscillation was analyzed from the theory of locally active and the edge of chaos [34]. Jin et al. proposed voltage-controlled locally active memristors with two pinched hysteresis loops and limited locally active ranges and applied the memristor in a simple circuit which can generate chaotic attractor [35]. Chang et al. proposed a bi-stable locally active memristor with twin symmetrical locally activity ranges and applied it in an oscillator system to analyze the dynamics of memristor [36]. Mannan et al. proposed a 4-lobe Chua's corsage memristor with three pinched hysteresis loops and limited locally active ranges; they analyzed the phenomenon of the edge of chaos [37]. Wang et al. proposed a locally active memristor with two pinched hysteresis loops and four locally active regions. The effect of locally active memristors on the complexity of systems was discussed [38]. Tang and Wang proposed a locally active memristor with two pinched hysteresis loops and wide locally active regions and found that firing behaviors occur only within the locally active regions [39]. Lin et al. proposed a tri-stable locally active memristor with five locally active regions by which constructed 2D HR neurons could generate multiple firing patterns [40]. Ref. [41] proposed a locally active memristor with three pinched hysteresis loops and wide locally active regions by introducing polynomial functions into the equation of state.

In previous studies, the locally active memristor has only one to three stable pinched hysteresis loops. Only Ref. [42] proposed a multistable locally active memristor by which constructed neural networks could generate controllable multi-stable behavior.

However, it is worth noting that the fractional-order multistable locally active memristor has not been studied. Motivated by these considerations, a fractional-order multistable locally active memristor is proposed for the first time in this paper, and it has infinitely many coexisting pinched hysteresis loops and wide locally active regions. The effects of parameters on the nonvolatile and multistable characteristics of the memristor are investigated. Through analysis, we find that the fractional-order memristor has stronger locally active and memory characteristics and wider nonvolatile ranges than the integer-order memristor. Furthermore, this fractional-order multistable locally active memristor is applied in a simple chaotic system. It is found that oscillations occur only within the locally active regions. Through the theoretical and numerical analysis, it is found that the fractional-order system not only has complex dynamics but also presents two phenomena that have not been found in other chaotic systems; these phenomena are called transient transition and state jump.

The rest of this paper is organized as follows: Section 2 introduces the mathematical model of fractional-order multistable locally active memristor and uses the power-off plot (POP) and DC v-i Loci to verify the nonvolatile, multistable and locally active characteristics of this memristor. In Sect. 3, a fractional-order chaotic system based on this fractional-order multistable locally active memristor is established and the nonlinear dynamics of this system are numerically

revealed using bifurcation diagrams, Lyapunov exponent spectrum and phase portraits. In Sect. 4, the circuit simulation is carried out by PSIM to verify the validity of the numerical simulation results. Section 5 summarizes this paper.

2 Fractional-order multistable locally active memristor

2.1 The fractional-order multistable locally active memristor model

Fractional calculus generalizes traditional calculus to non-integer integrals and differentials [43]. In this paper, we consider using Caputo's definition to obtain fractional derivatives [44]. So, the fractional-order derivative of $f(t)$ defines:

$$ {}_rD_t^{\alpha} f(t) = \frac{1}{\Gamma(n-\alpha)} \int_r^t \frac{f^{(n)}(\tau)}{(t-\tau)^{\alpha-n+1}} d\tau, \quad (n-1 < \alpha \le n) \tag{1} $$

where α ($\alpha \in (0, 1]$) is the fundamental operator of fractional calculus or called α-order, $\Gamma(.)$ is Gamma function.

Memristor can be regarded as a resistor whose resistance varies with the charge or the magnetic flux. According to the definition of memristor [42], a fractional-order multistable locally active memristor is proposed as follows:

$$ \begin{cases} {}_rD_t^{\alpha} x = -v + \sin(mx) \\ i = nxv \end{cases} \tag{2} $$

where i and v are the input current and input voltage, x is the state variable of the memristor, nx is the memductance and m and n are parameters.

To explore the effect of α-order on the characteristics of memristor, we can set parameters $m = 1, n = 1$ and consider that the memristor is driven by a sinusoidal signal source with amplitude A=1V and frequency $f = 3.14$ Hz. The larger the area of the hysteresis loop, the better the memory characteristics [25]. From the pinched hysteresis loops under different α-order shown in Fig. 1, it is found that with the increase in α-order, the area of pinched hysteresis loops decreases. So, the fractional-order multistable memristor has stronger memory characteristics than the integer-order multistable memristor [42]. In addition, the memductance can be expressed as the slope of pinched hysteresis loop [35]. From Fig. 1, it is found that the smaller the α-order, the greater the negative slope at the origin. Because the memristor is active when the memductance is less than 0, the fractional-order multistable memristor has stronger locally active characteristics than the integer-order multistable memristor [42].

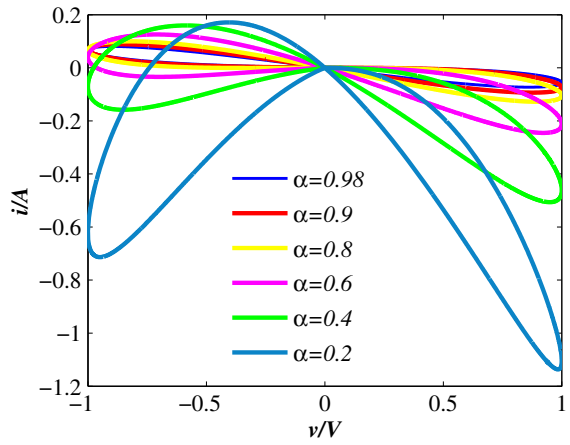

Fig. 1 Pinched hysteresis loop for different α-orders, when parameters $m = 1$ and $n = 1$

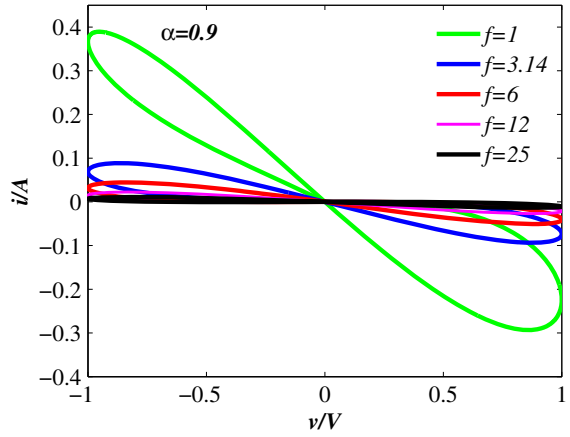

Fig. 2 Pinched hysteresis loop for different frequencies, when parameters $m = 1$, $n = 1$ and $\alpha = 0.9$

To explore the effect of frequency on the memristor, we can set parameters $m = 1, n = 1$ and $\alpha = 0.9$. The memristor is driven by a sinusoidal signal source with amplitude A = 1V at different frequencies. From Fig. 2, it is found that with the increase of frequencies, the area of pinched hysteresis loops decreases and gradually approaches a single-valued function.

2.2 Nonvolatile and multistable

Nonvolatile characteristics allow memristor to retain memory when powered off and it can be proved by POP curve [33]. If the POP curve intersects the x-axis at two or more points with a negative slope, the fractional-order memristor is nonvolatile. When the memristor is powered off, the dynamical trajectory of the memristor must tend to the corresponding stable equilibrium point which means the multistability of memristor [42]. When the memristor is powered off, the input voltage $v = 0$. From Eq. (3), the state variable of the memristor becomes:

$$ {}_rD_t^{\alpha} x = \sin(mx) \tag{3}$$

From Eq. (3), we know ${}_rD_t^{\alpha} x$ intersects the x-axis at these points $x_e = k\pi/m$, where $k \in$z. And when $k = 2i + 1$, where $i \in$z, the slopes at x_e are negative, so x_e are stable equilibrium points. And when $k = 2i + 2$, x_e are unstable equilibrium points. Therefore, the attraction domains of $x_{stable} = (2i + 1)\pi/m$ are $(2i\pi/m, (2i + 2)\pi/m)$. Assuming that the nonvolatile ranges of x_{stable} are the length of attraction domains, the expression of nonvolatile ranges is described as follows:

$$ \mathrm{L_{pop}} = (2i + 2)\pi/m - 2i\pi/m = 2\pi/m \tag{4}$$

From Eqs. (3, 4), we know parameter m determines the location and the nonvolatile ranges of x_{stable}. The smaller the parameter m, the wider the nonvolatile ranges. When parameter m <1, the fractional-order memristor has wider nonvolatile ranges than the integer-order memristor [42].

Setting parameters $m = 0.5, n = 1$ and $\alpha = 0.9$, from Eq. (3), we can draw the POP curve shown in Fig. 3. It is found that ${}_rD_t^{\alpha} x$ intersects the x-axis at nine points in which $Q{-}2(-6\pi, 0)$, $Q_{-1}(-2\pi, 0)$, $Q_0(2\pi, 0)$, $Q_1(6\pi, 0)$ have negative slope, so they are stable, therefore the memristor is nonvolatile. When v_m=sin(6.28πt), Fig. 4 shows the coexisting pinched hysteresis loops under different initial states. It is found that when $x_0 = -6\pi$, the slope at the origin of the light black curve tends to -6π, which is memductance when the memristor is powered off [36]. When $x_0 = -2\pi$, the slope at the origin of the blue curve tends to -2π. When $x_0 = 2\pi$, the slope at the origin of the green curve tends to 2π. When $x_0 = 6\pi$, the slope at the origin of the black curve tends to 6π. The larger the initial value x_0 ranges, the more coexisting pinched hysteresis, so the fractional-order locally active memristor is multistable.

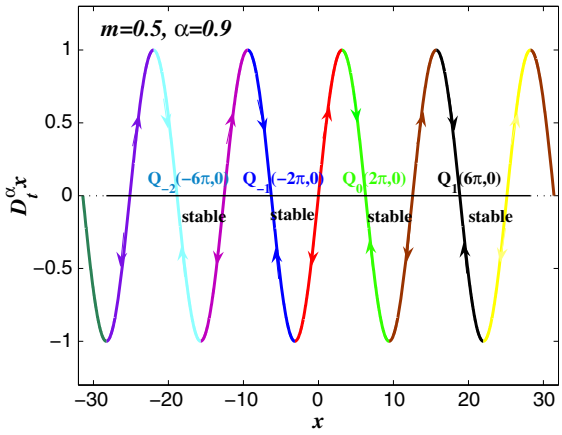

Fig. 3 POP curve of the memristor, when parameters $m = 0.5$, $n = 1$ and $\alpha = 0.9$

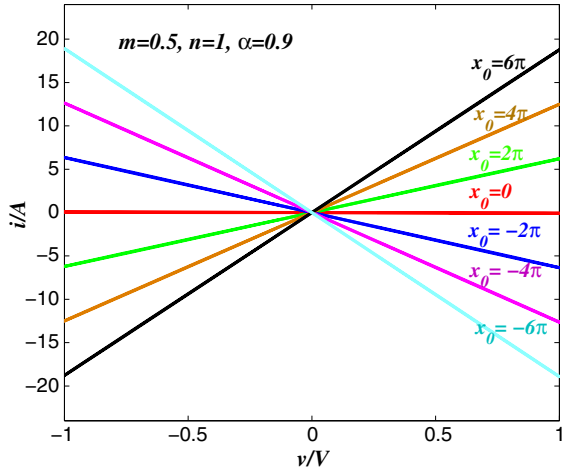

Fig. 4 Coexisting pinched hysteresis loops, when parameters $m = 0.5, n = 1$ and $\alpha = 0.9$

2.3 Wide locally active regions

DC voltage–current analysis can judge whether the memristor is locally active. If the DC v-i Loci has a negative slope, memristor is locally active [36]. To verify the locally active characteristic of fractional-order memristor, setting ${}_rD_t^{\alpha} x = 0$, Eq. (2) can be written as follows:

$$ \begin{cases} v = \sin(mx) \\ i = nxv \end{cases} \tag{5}$$

Setting $x \in(-10, 8], m = 1$ and $n = 1$, from Eq. (5), we can draw the DC v-i Loci shown in Fig. 5. It is found that the slope of the four curves of dark, purple, green and part of red is negative, so the memristor is locally

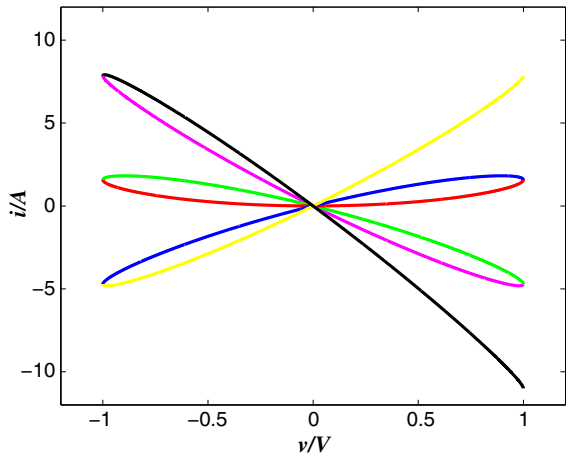

Fig. 5 Locally active ranges when $x_0 \in -10, 8]$, parameters $m = 0.5$ and $n = 1$

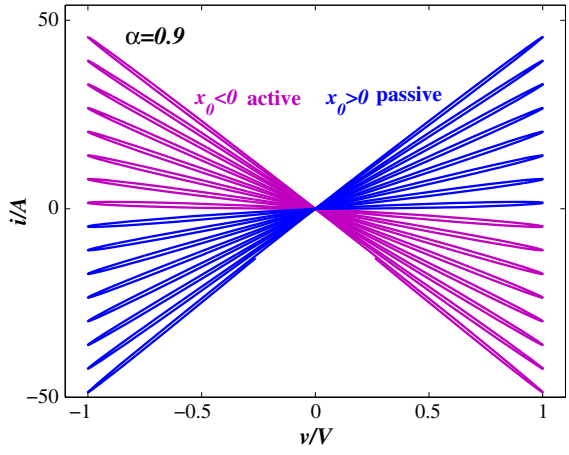

Fig. 6 Locally active ranges when $x_0 \in -50, 50]$, parameters $m = 1$, $n = 1$ and $\alpha = 0.9$

active. Extending the range of x, we can draw Fig. 6 which shows these purple curves drawn in $x_0 < 0$ have negative slopes. So, the whole part of $x_0 < 0$ is active. In conclusion, the fractional-order multistable memristor has wide locally active regions.

Through the above discussion, it is found that the fractional-order multistable locally active memristor not only has infinitely many coexisting pinched hysteresis loops and wide locally active regions but also has stronger locally active and memory characteristics and wider nonvolatile ranges than the integer-order memristor [42].

3 Fractional-order multistable locally active memristive chaotic system

3.1 A 4D fractional-order multistable locally active memristive chaotic system model

From Poincare–Bendixson theory, if an autonomous system generates chaos, its equations satisfy at least three variables and one nonlinear term. J. Kengne et al. proposed a 3D simple autonomous jerk chaotic system with a cubic term which is described as follows [45]:

$$\begin{cases} \frac{dx}{dt} = y \\ \frac{dy}{dt} = az \\ \frac{dz}{dt} = x - by - z - x^3 \end{cases} \tag{6}$$

The fractional-order memristor described in Eq. (2) can be applied in system (6). After doing fractional calculus, a new 4D fractional-order memristive chaotic system is established as follows:

$$\begin{cases} D_t^\alpha x = y \\ D_t^\alpha y = az \\ D_t^\alpha = 2x - by - z + nyu - x^3 \\ D_t^\alpha u = -y + \sin(mu) \end{cases} \tag{7}$$

where u denotes the state variable of memristor, a, b, m and n are the parameters. And $\alpha \in (0,1]$, when $\alpha = 1$, system (7) becomes an integer-order chaotic system.

Setting the left-hand side of Eq. (7) to 0, it is found that whatever parameters a, b and n are, system (7) has three types of equilibrium points which are $(0, 0, 0, k\pi/m)$, $(\sqrt{2}, 0, 0, k\pi/m)$ and $-\sqrt{2}, 0, 0, k\pi/m)$, where $k \in$z.

3.2 Stability analysis of equilibrium points

For simplicity, these three types of equilibrium points are described as $E_{x_0} = (x_0, 0, 0, k\pi/m)$. When $x_0 = 0$, we can obtain the first type of equilibrium point $E_{x_0} = E_{1k} = (0, 0, 0, k\pi/m)$, when $x_0 = \sqrt{2}$, we can obtain the second type of equilibrium point $E_{x_0} = E_{2k} = (\sqrt{2}, 0, 0, k\pi/m)$, and when $x_0 = -\sqrt{2}$, we can obtain the third type of equilibrium point $E_{x_0} = E_{3k} = (-\sqrt{2}, 0, 0, k\pi/m)$.

The Jacobian matrix of system (7) at E_{x_0} is obtained as follows:

$$J_\Sigma = \begin{pmatrix} 0 & 1 & 0 & 0 \\ 0 & 0 & a & 0 \\ 2-3x_0^2 & -b+nk\pi/m & -1 & 0 \\ 0 & -1 & 0 & m\cos(k\pi) \end{pmatrix} \tag{8}$$

The characteristic polynomial of the Jacobian matrix (8) is described as follows:

$$(m\cos(k\pi)-\lambda)\left[\lambda^3+\lambda^2+(ab-ank\pi/m)\lambda + \left(3ax_0^2-2a\right)\right]=0 \tag{9}$$

Lemma 1 [46]: The fractional-order nonlinear system

$$D_t^\alpha X = f(X), 0<\alpha\le 1 \tag{10}$$

is asymptotically stable at the equilibrium E (x_0, y_0, z_0, u_0), if all eigenvalues λ of Jacobian matrix J_E satisfy the condition:

$$|\arg(\lambda)| > \frac{\alpha\pi}{2} \tag{11}$$

where $X=(x,y,z,u)^T$, $f(X)=[f_1(x), f_2(x), f_3(x), f_4(x)]^T$, $f_i(X)=f_i(x,y,z,u)(i=1,2,3,4)$ and $\arg(\lambda)$ is the principal argument of eigenvalue λ.

Whatever parameters a, b and n are, Eq. (9) have a fixed solution $\lambda_1=\cos(k\pi)=\pm 1/m$. Take roots λ_1 out of Eq. (9); the rest part of characteristic polynomial can be described as follows:

$$\lambda^3+\lambda^2+(ab-ank\pi/m)\lambda+\left(3ax_0^2-2a\right)=0 \tag{12}$$

Assuming that the roots of Eq. (12) are λ_2, λ_3 and λ_4. To obtain the stability of equilibrium points, the characteristic roots of Eq. (12) are discussed as follows:

(i)According to the criterion of Routh–Hurwitz, λ_2, λ_3 and λ_4 all have negative real parts, when the following inequalities are true.

$$a_1>0, a_1a_2-a_3>0, a_3(a_1a_2-a_3)>0 \tag{13}$$

where a_1, a_2 and a_3 denote the coefficients of λ_2, λ and constant term in Eq. (12), so we can obtain $a_1=1$, $a_2=ab-ank\pi/m$ and $a_3=3ax_0^2-2a$, and expression (13) can be simplified as follows:

$$\begin{cases} b-nk\pi/m+2-3x_0^2>0 \\ \left(3x_0^2-2\right)\left(b-nk\pi/m+2-3x_0^2\right)>0 \end{cases} \tag{14}$$

If expression (14) is true, λ_2, λ_3 and λ_4 all have negative real parts.

(ii)When $E_{x_0}=E_{1k}$=(0, 0, 0, $k\pi/m$), substituting $x_0=0$ into expression (14), expression (15) is obtained.

$$\begin{cases} b-nk\pi/m+2>0 \\ -2(b-nk\pi/m+2)>0 \end{cases} \tag{15}$$

If expression (15) is true, λ_2, λ_3 and λ_4 all have negative real parts, and E_{1k} is stable. However, the first inequality of expression (15) contradicts the second inequality, so whatever a, b, m and n are, λ_2, λ_3 and λ_4 have at least one positive real part. According to the Vieta theorem of cubic equation, we know $\lambda_2\lambda_3\lambda_4=-a_3=2a>0$, $\lambda_2+\lambda_3+\lambda_4=-a_1=-1<0$, so the roots of Eq. (12) at E_{1k} are a positive real root and a pair of conjugated complex roots whose real parts are negative, so E_{1k} is the saddle-focus point of index 1.

(iii)When $E_{x_0}=E_{2k,3k}$=($\pm\sqrt{2}$, 0, 0, $k\pi/m$), substituting $x_0=\pm\sqrt{2}$ into expression (14), expression (16) is obtained.

$$\begin{cases} b-nk\pi/m-4>0 \\ 4(b-nk\pi-4)>0 \end{cases} \tag{16}$$

When $b>nk\pi/m+4$, expression (16) is true, so whatever parameter a is, λ_2, λ_3 and λ_4 all have negative real part, and $E_{2k,3k}$ are stable equilibrium points. When $b<nk\pi/m+4$, expression (16) is not true, so whatever parameter a is, λ_2, λ_3 and λ_4 have at least one positive real part. According to the Vieta theorem of cubic equation, we know $\lambda_2\lambda_3\lambda_4=-a_3=-4a<0$, $\lambda_2+\lambda_3+\lambda_4=-a_1=-1<0$, so the roots of Eq. (12) at $E_{2k,3k}$ are a negative real root and a pair of conjugated complex roots whose real parts are positive. By Lemma 1, the stability of $E_{2k,3k}$ is related to α-order. When $|\arg(\lambda)|>\alpha\pi/2$, we can know $E_{2k,3k}$ are asymptotically stable, otherwise, unstable. The above discussion can be concluded in Table 1.

3.3 Numerical illustrations

To better prove the correctness of the above discussion, we make numerical illustrations. Setting parameters $a=3.5, b=0.8, m=1$ and $n=0.2$, from expression (16), we can divide k into two cases. Case 1: when $0.2k\pi+4<0.8$, we can obtain $k<-5.093$, and expression (16) is true. This case corresponds to Number I of Table 1. Case 2: When $0.2k\pi+4>0.8$, we can obtain $k>-5.093$, and expression (16) is not true. This case corresponds to Number II of Table 1. The roots of Eq. (12) are shown in Table 2 which are consistent with the

Table 1 The eigenvalues and stabilities of equilibrium points

Number	b	$\lambda_2(E_{1k})$	$\lambda_{3,4}(E_{1k})$	Stability of equilibrium	$\lambda_2(E_{2k,3k})$	$\lambda_{3,4}(E_{2k,3k})$	Stability of equilibrium
I	$b > nk\pi/m+4$	>0	$-p \pm q$i	Unstable	$-p \pm q$i	$-p \pm q$i	Stable
II	$b < nk\pi/m+4$	>0	$-p \pm q$i	Unstable	<0	$p \pm q$i	α-related

Table 2 The numerical simulation results of equilibrium point stability

k	$\lambda_2(E_{1k})$	$\lambda_{3,4}(E_{1k})$	Stability of equilibrium	$\lambda_2(E_{2k,3k})$	$\lambda_{3,4}(E_{2k,3k})$	Stability of equilibrium
$k=-1$	1	-1 ± 2.449i	Unstable	-2	0.5 ± 2.597i	When α <0.878, stable. α >0.878, saddle-focus points of index 2
$k=-5$	0.482	-0.741 ± 3.736i	Unstable	-1.013	0.689 ± 3.716i	When α <0.83, stable. α >0.83, saddle-focus points of index 2
$k=-6$	0.421	-0.711 ± 4.011i	Unstable	-0.881	-0.594 ± 3.985i	Stable
$k=-7$	0.374	-0.687 ± 4.270i	Unstable	-0.776	-0.111 ± 4.243i	Stable

results in Table 1, so the above discussion is correct. When $k=-5, 1$, the stability of $E_{2k,3k}$ is related to α. By Lemma 1, the results are proved as follows:

When $|\frac{Im(\lambda_{3,4})}{Re(\lambda_{3,4})}| > tan(\frac{\alpha\pi}{2})$, $E_{2k,3k}$ are asymptotically stable. When $|\frac{Im(\lambda_{3,4})}{Re(\lambda_{3,4})}| = tan(\frac{\alpha\pi}{2})$, Hopf bifurcation is generated [47]. When $|\frac{Im(\lambda_{3,4})}{Re(\lambda_{3,4})}| < tan(\frac{\alpha\pi}{2})$, $E_{2k,3k}$ are unstable. The above discussion can be concluded in Table 2.

3.4 Complex nonlinear dynamic analysis

Bifurcation analysis, phase diagrams and Lyapunov exponents are used to explore the nonlinear dynamics of system (7).

3.4.1 Oscillation only in locally active regions

Based on Sec. 2.3, when the initial states of the memristor less than 0, the fractional-order multistable memristor is locally active. In Eq. (7), u denotes the state variable of the memristor, u_0 denotes the initial states of the memristor. The bifurcation diagram about u_0 is plotted in Fig. 7a with the fixed parameters $a = 3.5$, $b = 0.8$, $n = 0.2$, $m = 1$ and $\alpha = 0.96$. System (7) exhibits completely different oscillation behaviors on either side of $u_0 = 0$. When $u_0 < 0$, the memristor is active and the system is chaotic. When $u_0 > 0$, the memristor is negative and the system cannot oscillate.

The bifurcation diagram about parameter a is plotted in Fig. 7b with the fixed parameters $b = 0.8$, $n = 0.2$, $m = 1$ and $\alpha = 0.96$. The blue curve corresponds to the initial value (0.1, 0.1, −0.1, −0.3), where system (7) exhibits complex oscillation behaviors. The red curve corresponds to the initial value (0.1, 0.1, −0.1, 0.3), where system (7) exhibits static behavior. These simulation results suggest that oscillations only occur in the locally active regions.

3.4.2 Asymptotically periodic oscillations

Theorem 1 [48]: The autonomous fractional-order differential equations

$$D^{\alpha} x_i(t) = f_i(x_1(t), x_2(t), \ldots x_n(t)), i = 1, 2, \ldots, n \quad (17)$$

with $0 < \alpha < 1$ and f_i being some nonlinear function, which cannot have any non-constant exact smooth periodic solution. The same is true for non-autonomous fractional systems [49].

From Theorem 1, we know that fractional-order systems cannot have exact periodic solutions. However, according to Ref. [50], when the trajectory of fractional-order system shown in Eq. (17) satisfies $\lim_{t\to+\infty} x_i(t+T)-x_i(t)=0$, $i = 1, 2, ...,$ n and T>0, we call it "asymptotically T-periodic oscillations". In the real case, t tends to infinity means that t tends to a larger number.

From many numerical simulations [50–53], we can observe the existence of asymptotically periodic oscillations, for example, Fig. 9 in Ref. [50], Fig. 11 in Ref. [51], Figs. 6, 7 in Ref. [52] and Fig. 2 in Ref. [53]. Besides, in this paper, we also can find the existence of asymptotically periodic oscillation. For example:

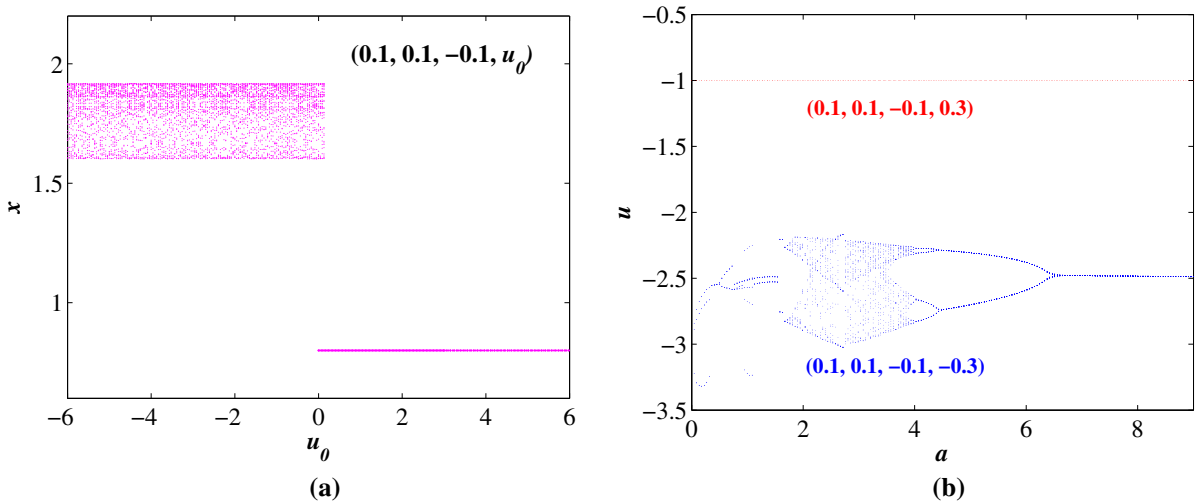

Fig. 7 **a** Bifurcation diagram for u_0. **b** Bifurcation diagram for parameter a with initial value (0.1, 0.1, −0.1, −0.3) (blue curve) and (0.1, 0.1, −0.1, 0.3) (red curve)

For system (7), the predictor–corrector Adams–Bashforth–Moulton in Ref. [54] is used to solve the fractional-order differential equation. Setting parameters $a = 3.5$, $b = 0.8$, $n = 0.2$, $m = 1$, α as 0.9 and 0.95, respectively, initial value (0.1, 0.1, −0.1, 0) and the step length of simulation as 0.02, Fig. 8 can be obtained. From Fig. 8a, we know $\lim_{t\to t_m} \mathrm{x}(t+\mathrm{T})-\mathrm{x}(t)=0$, and from Fig. 8c, we know $\lim_{t\to t_n} \mathrm{x}(t+2\mathrm{T})-\mathrm{x}(t)=0$. In conclusion, we know that system (7) has asymptotically periodic 1 cycles shown in Fig. 8b and asymptotically periodic 2 cycles shown in Fig. 8d. For the convenience of writing, the word "Asymptotically periodic" is simplified as "A-period".

3.4.3 Lyapunov exponents and bifurcation analysis

Lyapunov exponents are used to exploring whether a system is in a chaotic state and bifurcation analysis can study the characteristics of a nonlinear system [39]. The method of Ref. [53] is used to solve the Lyapunov exponents. Setting parameters $a = 3.5$, $b = 0.8$, $n = 0.2$ and $m = 1$, Figure 9 shows the bifurcation diagram and the Lyapunov exponent spectrum for α-order. From the blue curve shown in Fig. 9a, it is found that when $\alpha \in (0, 0.878)$, system (7) is stable. When $\alpha = 0.878$, system (7) experiences Hopf bifurcation. When $\alpha \in (0.878, 0.943)$, A-period-1 bifurcation occurs. When $\alpha \in (0.943, 0.954)$, A-period-2 bifurcation occurs. When $\alpha \in (0.954, 1)$, chaos occurs.

Similarly, setting parameters $\alpha = 0.96$, $b = 0.8$, $n = 0.2$ and $m = 1$, Figure 10 shows the bifurcation diagram and the Lyapunov exponent spectrum for parameter a. From Fig. 10, it is found that when parameter $a \in (0.5, 1.5)$, A-period-1 bifurcation occurs. When parameter $a \in (1.5, 1.8)$, A-period-2 bifurcation occurs. When parameter $a \in (1.8, 4)$, chaos occurs. When parameter $a \in (4, 6.3)$, A-period-2 bifurcation occurs. And when parameter $a > 6.3$, A-period-1 bifurcation occurs.

3.4.4 Multistability analysis

If a nonlinear system displays three or more coexisting attractors under different initial values, the system is multistable [55]. Multistability reflects the sensitivity of the system to initial value. Setting parameters $a = 3.5, b = 0.8, n = 0.2$ and $m = 1$, after neglecting some of initial time, we can draw Fig. 11. Figure 11a shows the coexistence of two A-period-1 cycles and one stable point in the system when $\alpha = 0.9$. Figure 11b shows the coexistence of one A-period-1 cycle and A-period-2 cycle and one stable point in the system when $\alpha = 0.9448$. Figure 11c shows the coexistence of two single scrolls and A-period-1 cycle in the system when $\alpha = 0.975$. Figure 11d shows the coexistence of two double-scrolls and A-period-1 cycle in the system when $\alpha = 0.99$. From Fig. 9a, we also can see the multistability of system (7) . See Table 3 for details.

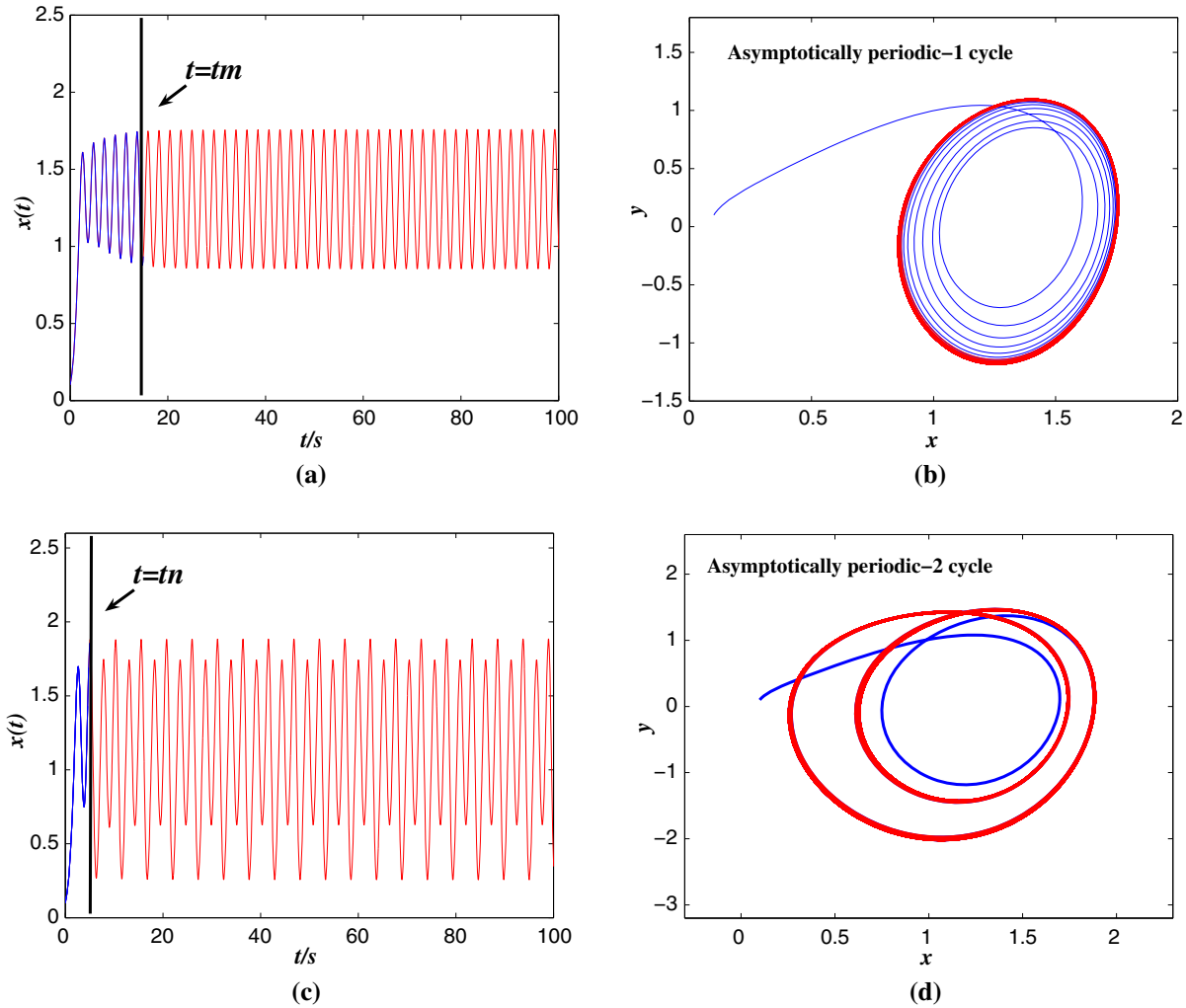

Fig. 8 **a** The timing diagrams of the system (7) when α is 0.9. **b** The phase diagrams of system (7) when α is 0.9. **c** The timing diagrams of the system (7) when α is 0.95. **d** The phase diagrams of system (7) when α is 0.95

3.4.5 Transient transition

In this paper, we can find two new phenomena: transient transition and state jump. And the trajectories of these two phenomena are different from the asymptotically periodic oscillation mentioned in Sect. 3.4.2.

When the trajectory of system (7) satisfies that in some local time regions, the trajectory appears as period, while in the nearby regions outside of these local time regions, the trajectory shows aperiodic oscillation, we call it "local periodic oscillation". That is, when $t \in (t_a, t_b)$, $x(t+T)-x(t)=0$, while when $t \in (t_a-\delta, t_a)$ and $t \in (t_b, t_b+\delta)$, $x(t+T)-x(t)\neq 0$, where δ is a very small positive number.

Similarly, when the trajectory of system (7) satisfies that in some local time regions, the trajectory appears as chaos, while in the nearby regions outside of these local time regions, the trajectory shows non-chaotic oscillation, we call it "local chaos". That is, when $t \in (t_a, t_b)$, the trajectory appears as chaos, while when $t \in (t_a-\delta, t_a)$ and $t \in (t_b, t_b+\delta)$, the trajectory appears as non-chaos.

Setting parameters $a = 3.5$, $b = 0.8$, $n = 0.2$, $m = 1$, $\alpha = 0.987$, initial value $(0.1, 0.1, -0.1, 0)$, the step length of simulation as 0.05 and the simulation time as (0s, 15000s) (these conditions must be strictly met), we can see this new phenomenon of transient transition

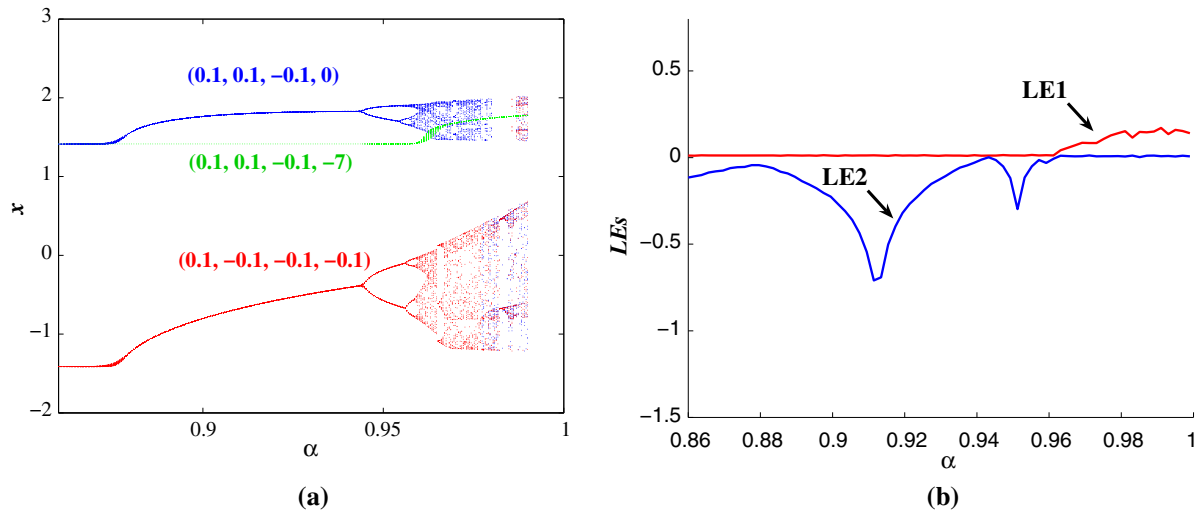

Fig. 9 **a** Bifurcation diagram for α with initial values (0.1, 0.1, −0.1, 0) (blue curve), (0.1, −0.1, −0.1, −0.1) (red curve) and (0.1, 0.1, −0.1, −7) (green curve). **b** Lyapunov exponent spectrum for initial values (0.1, 0.1, −0.1, 0)

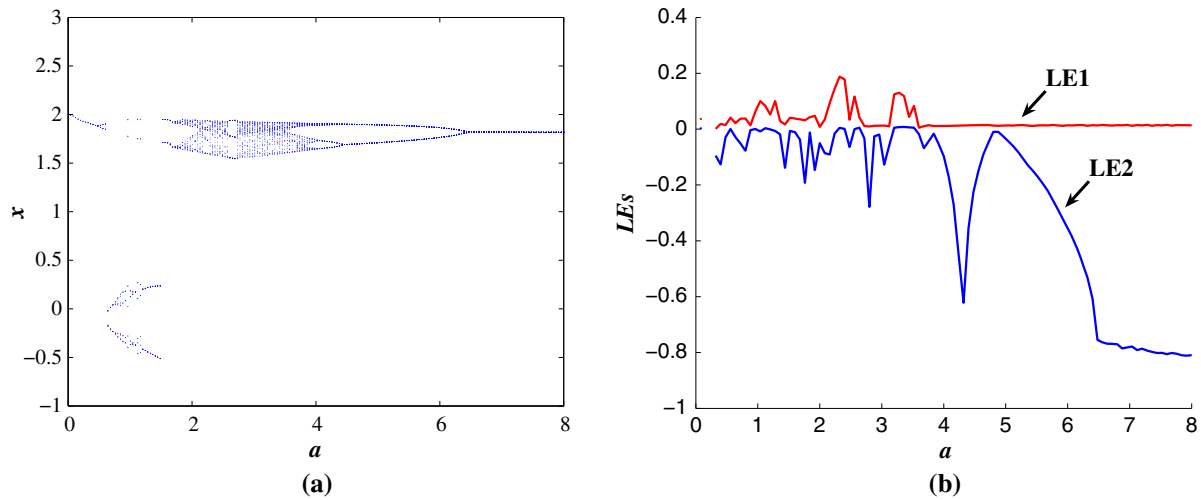

Fig. 10 **a** Bifurcation diagram for parameter a with initial values (0.1, 0.1, −0.1, 0). **b** Lyapunov exponent spectrum for parameter a with initial values (0.1, 0.1, −0.1, 0)

which has not been found in any other integer-order or fractional-order chaotic system.

From Fig. 12, we can see system (7) produces local periodic oscillation, when $t \in$(50s, 2000s). The local periodic oscillation transfers to local chaos, when $t = 2000$s. The local chaos transfers to local periodic oscillation, when $t = 2828$s. After that, local chaos and local periodic oscillation transition alternately appear. Figure 13 shows the local chaos, when $t \in$(1100s, 1400s), and system (7) generates local double-scroll chaotic attractor. Figure 14 shows the local periodic oscillation, when $t \in$(1800s, 2200s), and system (7) generates local period-2 cycle.

3.4.6 State jump

Setting parameters $a = 1$, $b = 0.8$, $n = 0.2$, $m = 1$, $\alpha = 0.96$ and the step length of simulation as 0.02, from Eq. (12), we can obtain the roots of E_1 are $\lambda_1 = 0.7378$, $\lambda_{2,3} = -0.8689 \pm 1.3984$i, so E_1 is the saddle-focus

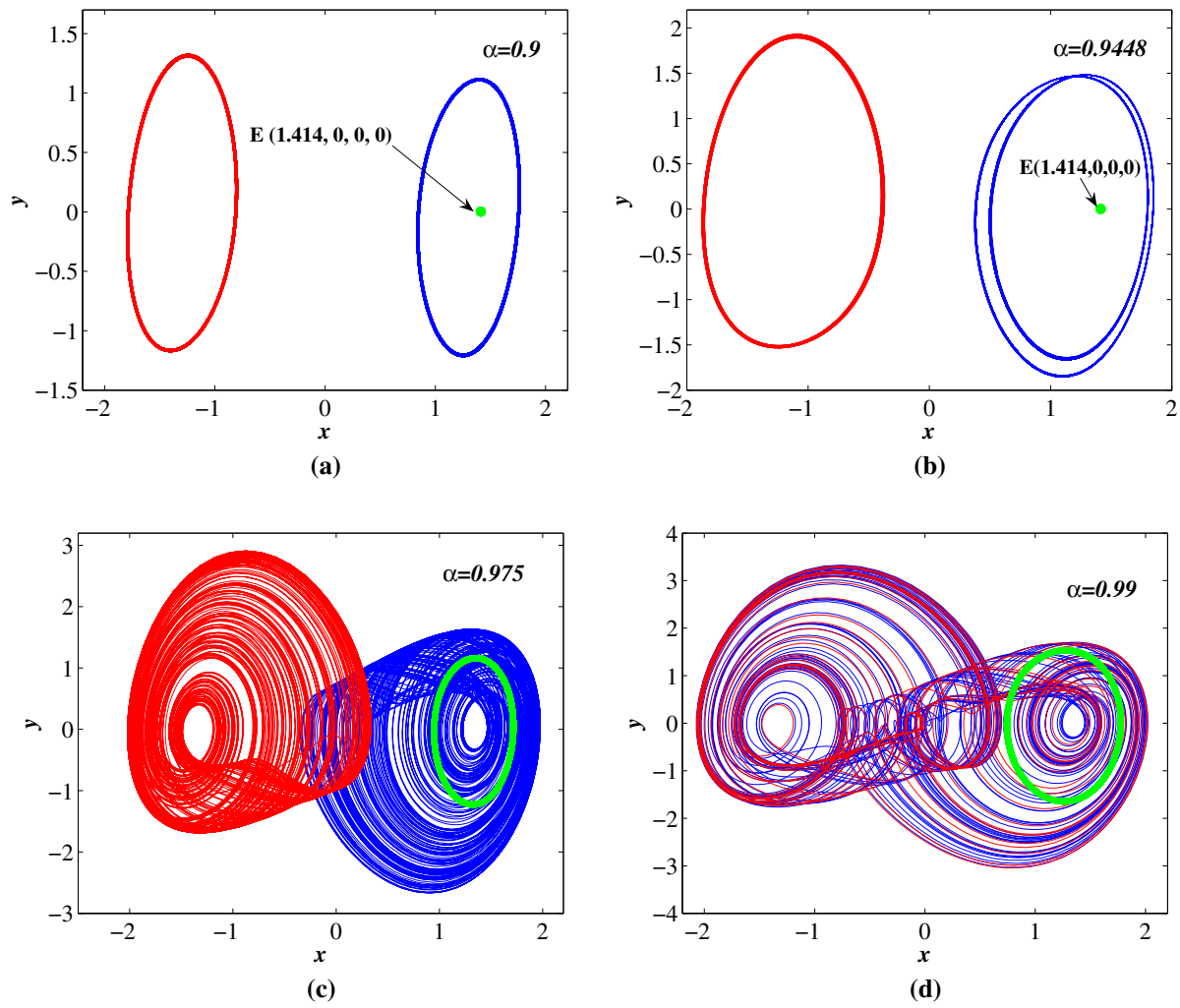

Fig. 11 Phase portraits for different α with initial values (0.1, 0.1, −0.1, 0) (blue curve), (0.1, −0.1, −0.1, −0.1) (red curve) and (0.1, 0.1, −0.1, −7) (green curve) (**a**) $\alpha = 0.9$ (**b**) $\alpha = 0.9448$ (**c**) $\alpha = 0.975$ (**d**) $\alpha = 0.99$

point of index 1. The roots of $E_{2,3}$ are $\lambda_1 = -1.629$, $\lambda_{2,3} = 0.3148 \pm 0.3148i$. From Lemma 1, we know when $\alpha < 0.8712$, $E_{2,3}$ are stable. When $\alpha > 0.8712$, $E_{2,3}$ are saddle-focus points of index 2. In brief, when $\alpha = 0.96$, E_1 is the saddle-focus point of index 1, $E_{2,3}$ are saddle-focus points of index 2. In Ref. [55], the saddle-focus points of index 2 are important for generating chaos. Usually, scrolls are generated around the saddle focus points of index 2, and the saddle-focus points of index 1 are responsible only for connecting the scrolls.

However, from Fig. 15, it is found that the results are different from the viewpoint in Ref. [55]. According to the descriptions of local chaos and local period, after neglecting some of initial time, Fig. 15a shows system (7) produces a new oscillation: local period-4 oscillation jumps to local period-2 oscillation alternately when $t \in (20s, 200s)$. Figure 15b, c shows that local period-4 cycle and local period-2 cycle are coupled together, the local period-4 cycle is produced by E_2, the local period-2 cycle is produced by E_3, and E_1 generates the spool to connect them. This phenomenon has not been found in other fractional-order or integer-order chaotic systems, we call it state jump.

Similarly, setting parameters $a = 1$, $b = 0.8$, $n = 0.2$, $m = 1$ and $\alpha = 0.97$, we can draw Fig. 16. Figure 16a shows that local chaos jumps to local period-2 oscillation alternately when $t \in (20s, 400s)$. Figure 16b, c shows that the local chaotic attractor and

Table 3 The coexisting attractors under different α-order

α-order	Steady states
k= (0, 0.875)	Three stable points
k= (0.875, 0.880)	Two stable points and A-period-1 cycle
k= (0.880, 0.943)	Two A-period-1 cycles and one stable point
k= (0.943, 0.945)	One A-period-1 cycle, A-period-2 cycle and one stable point
k= (0.945, 0.955)	Two A-period-2 cycles and one stable point
k= (0.955, 0.960)	Chaotic attractor, A-period-2 cycle and one stable point
k= (0.960, 1)	Two chaotic attractors and A-period-1 cycle

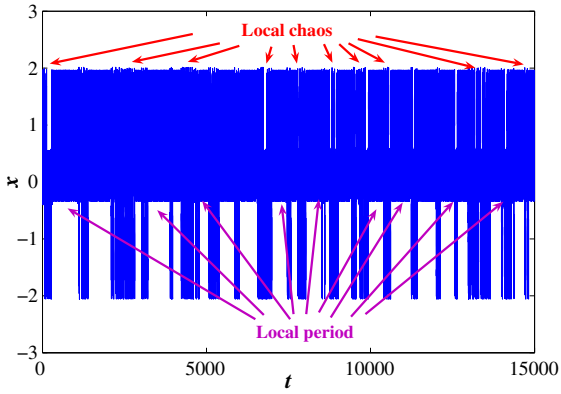

Fig. 12 Time-domain plot of $t \in (0, 15000s)$, when $a = 3.5$, $b = 0.8$, $n = 0.2$, $m = 1$, $\alpha = 0.987$, initial value (0.1, 0.1, −0.1, 0)

local period-2 cycle are coupled together. The local chaotic attractor is produced by E_2, the local period-2 cycle is produced by E_3, and E_1 generates the spool to connect them.

3.4.7 Anti-monotonicity

Interestingly, system (7) displays a full Feigenbaum tree. In other words, system (7) is anti-monotonicity. To prove this phenomenon, we can set parameters $n = 0.2$, $m = 1$, $\alpha = 0.96$ and initial value (0.1, 0.1, −0.1, 0). Parameter b is given as 1.1, 0.95, 0.935 and 0.88, and a is control parameter. The corresponding bifurcation diagrams are shown in Fig. 17a–d. System (7) generates the primary A-period-2 bubble, when $b = 1.1$. System (7) generates the primary A-period-4 bubble, when $b = 0.95$. System (7) generates the primary A-period-6 bubble, when b =0.935. System (7) generates a full Feigenbaum tree, when $b = 0.88$.

3.4.8 Comparison with other memristive chaotic systems

Many integer-order or fractional-order chaotic systems have been studied. To clarify the characteristics of the fractional-order multistable locally active memristive chaotic systems, we compare them with the ones in other papers. Table 4 shows the comparison results. From Table 4, the fractional-order system proposed in this paper not only has complex dynamics such as infinitely many discrete equilibrium points, multistability and anti-monotonicity but also presents two phenomena that have not been found in other chaotic systems: transient transition and state jump.

4 Circuit implementation

Fractional-order capacitance is the key to implement the fractional-order memristor and fractional-order chaotic circuit. In Refs. [58,59], the fractional-order capacitance C_q can be realized by the paralleled capacitance and resistance. See Table 5 for details.

We can implement the memristor circuit and memristive chaotic circuit by capacitors, resistors, operational amplifiers TL082CP, analog multipliers AD633JN and trigonometric function converters AD639AD.

In this paper, these special initial values, such as $\pm 6\pi$, $\pm 4\pi$ and $\pm 2\pi$, are difficult to obtain precisely by constantly switching the supply voltage in hardware circuits [57]. To accurately reveal the multistable characteristic and complex transient behavior depending on the initial conditions, PSIM version 9.0.3 software is employed for circuit simulation. That is because PSIM software not only provides the circuit elements needed for simulation, but also can easily set the initial values of inductance current and capacitance voltage. The process of setting the initial values: double-click the circuit element and input the required initial value in the "Initial" option box.

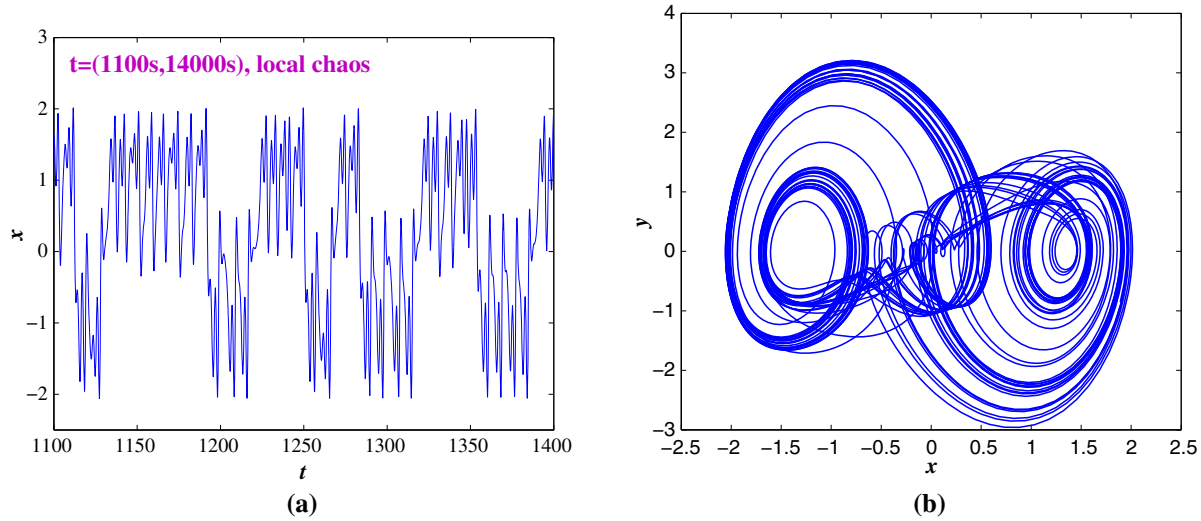

Fig. 13 **a** Time-domain plot of $t \in$(1100s, 1400s). **b** Phase portraits of $x - y$ axis $t \in$(1100s, 1400s)

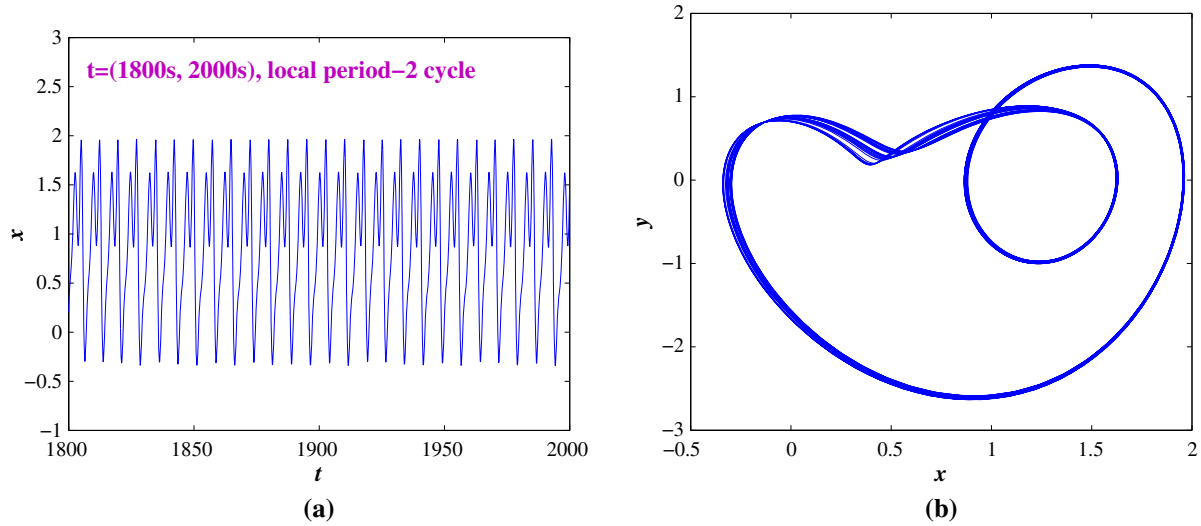

Fig. 14 **a** Time-domain plot of $t \in$(1800s, 2200s). **b** Phase portraits of $x - y$ axis $t \in$(1800s, 2200s)

4.1 Fractional-order multistable locally active memristor circuit implementation

From Eq. (2), the memristor circuit can be implemented. Figure 18 shows this memristor circuit schematic diagram. According to Kirchhoff's law, the circuital equations of the memristor can be described as follows:

$$\begin{cases} c_q \frac{d^q v_u}{dt^q} = \frac{-v}{R} + \frac{\sin(v_u)}{R} \\ i = v_u v \end{cases} \tag{18}$$

where q is the fractional order, v_u is memristor state and v and i are the input voltage and input current.

When v=sin(6.28πt), the pinched hysteresis loops shown in Fig. 19 can be obtained from the memristor circuit in PSIM simulation when q is fixed as 0.9, 0.98. We can see Fig. 19 is consistent with Fig. 1.

According to the voltage division formula of parallel capacitors, we know that the initial voltage of the fractional-order integrating capacitor C_q in Fig. 18 is equal to the sum of the initial voltages of the capacitors C_1, C_2 and C_3. Therefore, in PSIM software, when the inputting initial voltages for C_2 and C_3 are always 0V, the initial voltage of C_q is set by C_1 shown in Fig. 18.

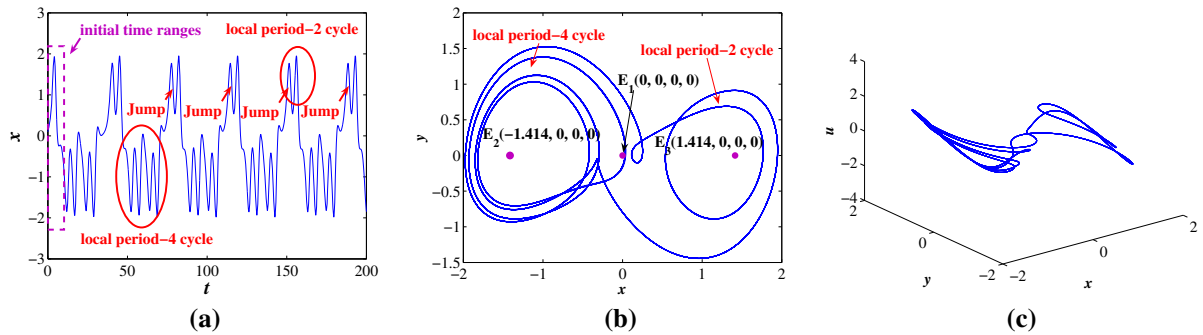

Fig. 15 After neglecting initial time ranges, when $t \in$(20s, 200s) local period-4 cycle jumps to local period-2 cycle **a** Time-domain plot. **b** Phase portraits of $x - y$ axis. **c** Phase portraits of $x - y - u$ axis

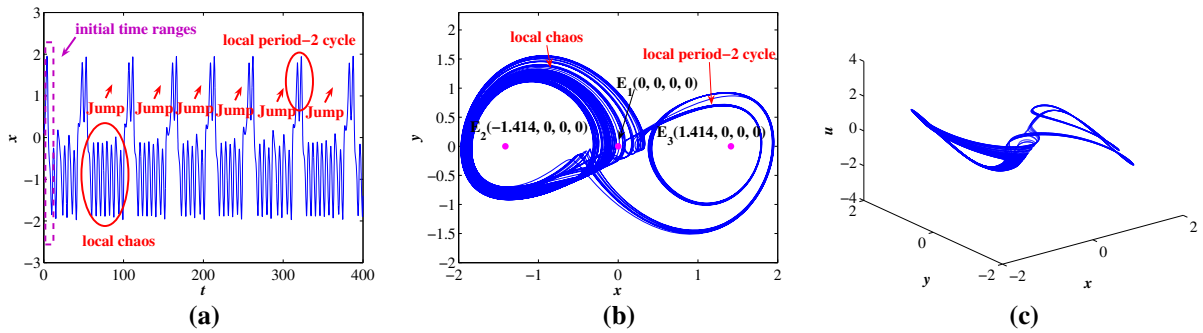

Fig. 16 After neglecting initial time ranges, when $t \in$(20s, 400s) local chaos jump to local period-2 cycle **a** Time-domain plot. **b** Phase portraits of $x - y$ axis. **c** Phase portraits of $x - y - u$ axis

When the inputting initial voltage for capacitor C_1 is -6π V, -4π V, -2π V, 0V, 2π V, 4π V and 6π V, the coexisting pinched hysteresis loops can be seen in Fig. 20, which are consistent with Fig. 4. So the simulation results are correct.

4.2 Fractional-order multistable locally active memristive chaotic system circuit implementation

From Eq. (7), the fractional-order memristive chaotic system circuit can be implemented. Figure 21 shows the fractional-order chaotic system circuit schematic diagram. According to Kirchhoff's law, the circuital equations can be described as follows:

$$\begin{cases} c_q \frac{d^q v_x}{dt^q} = \frac{v_y}{R} \\ c_q \frac{d^q v_y}{dt^q} = \frac{v_z}{Ra} \\ c_q \frac{d^q v_z}{dt^q} = -\frac{v_x^3}{R} + \frac{R_0 v_x}{R} - \frac{v_y}{R_b} + \frac{R_G v_z v_u}{R} - \frac{v_z}{R} \\ c_q \frac{d^q v_u}{dt^q} = -\frac{v_y}{R} + \frac{\sin(v_u)}{R} \end{cases} \tag{19}$$

When the initial voltages for other capacitors are always input at 0V, the initial values are set by C_{x1}, C_{y1}, C_{z1} and C_{u1} shown in Fig. 21.

Setting $R_a = 2.858\,\text{k}\Omega$, $R_b = 125\,\text{k}\Omega$, $R_G = 2\,\text{k}\Omega$ and $q = 0.9$, coexisting attractors can be obtained from the fractional-order chaotic system circuit in PSIM simulation. Figure 22a shows A-period-1 cycle, when the initial voltages of C_{x1}, C_{y1}, C_{z1} and C_{u1} are input to 0.1V, -0.1V, -0.1V and -0.1V, respectively. Figure 22b shows A-period-1 cycle, when the initial voltages of C_{x1}, C_{y1}, C_{z1} and C_{u1} are input to 0.1V, 0.1V, -0.1V and 0V, respectively. Figure 22c shows a stable point, when the initial voltages of C_{x1}, C_{y1}, C_{z1} and C_{u1} are input to 0.1V, 0.1V, -0.1V and -7V, respectively. Figure 22a–c is consistent with Fig. 11a, so the simulation results are correct.

Setting $R_a = 2.858\,\text{k}\Omega$, $R_b = 125\,\text{k}\Omega$, $R_G = 2\,\text{k}\Omega$, $q = 0.987$ and when the initial voltages of C_{x1}, C_{y1}, C_{z1} and C_{u1} are input to 0.1V, 0.1V, -0.1V and 0V, respectively, the behavior of transient transi-

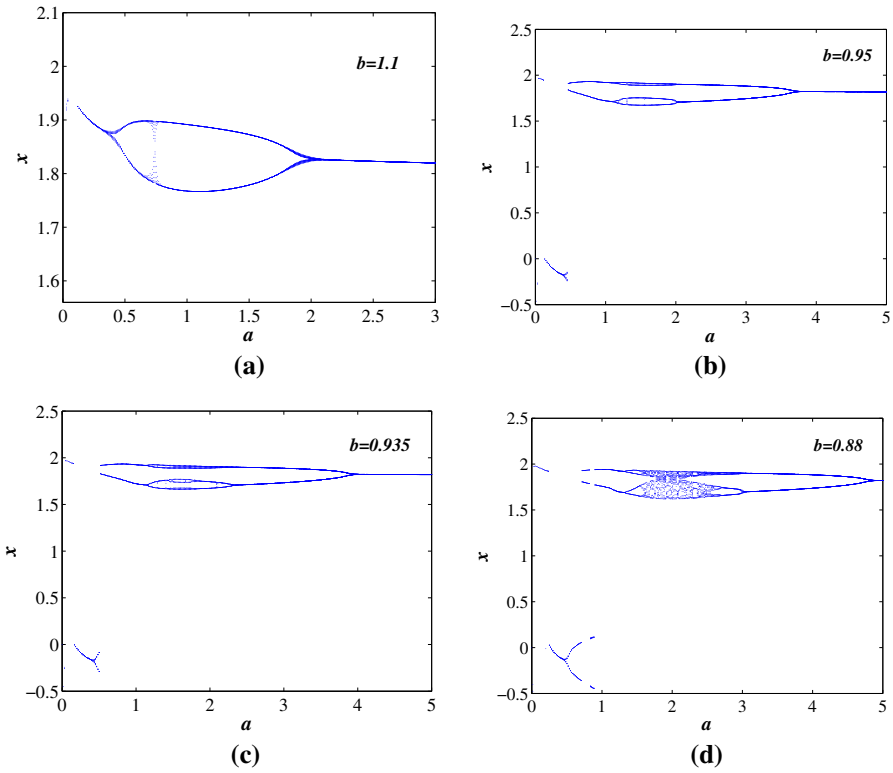

Fig. 17 Bifurcation diagrams of remerging Feigenbaum trees **a** A-period-2 bubble when $b = 1.1$. **b** A-period-4 bubble when $b = 0.95$. **c** A-period-6 bubble when b= 0.935. **d** Feigenbaum tree when $b = 0.88$

Table 4 The comparison with other memristive chaotic systems

References	Memristor	Equilibrium	Multistability	Hyperchaotic	Transient	State jump	Anti-monotonicity
Ref. [57]	Active	Line	Multistable	No	No	No	No
Ref. [56]	Locally active	Three	Bi-stable	No	No	No	No
This paper	Multistable locally active	Infinite	Multistable	No	Alternately	Yes	Yes

Table 5 Fractional-order capacitance C_q

q	$R_1(\Omega)$	$R_2(\Omega)$	$R_3(\Omega)$	$C_{(x,y,z,u)1}(\mu)$	$C_{(x,y,z,u)2}(\mu)$	$C_{(x,y,z,u)3}(\mu)$
0.9	68.84M	250k	2.5	1.232	1.835	1.1
0.97	87.0129M	85	–	1.0197	3.8042	–
0.98	91.187M	190.933	–	0.97582	3.68059	–
0.987	94.062M	397.646	–	0.9458	3.59924	–

tion can be obtained from the fractional-order chaotic system circuit in PSIM simulation. From Fig. 23, we can see the behavior of local chaos and local period transition alternately occurring and Fig. 23 is consistent with Fig. 12, so the simulation results are correct.

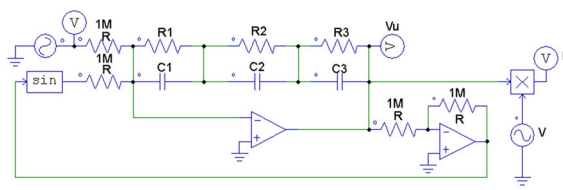

Fig. 18 Circuit configuration of the memristor

Setting $R_a = 10k\Omega$, $R_b = 125\,\mathrm{k}\Omega$, $R_G = 2\,\mathrm{k}\Omega$, $q = 0.97$ and when the initial voltages of C_{x1}, C_{y1}, C_{z1} and C_{u1} are input to 0.1V, 0.1V, -0.1V and 0V, respectively, the behavior of state jump can be obtained from the fractional-order chaotic system circuit in PSIM simulation. And Fig. 24 is consistent with Fig. 16b, so the simulation results are correct.

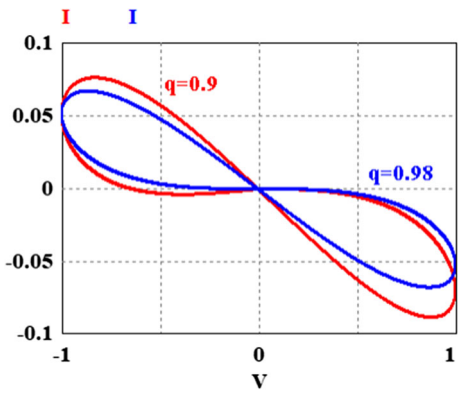

Fig. 19 Pinched hysteresis loops obtained from the memristor circuit in PSIM simulation when $q = 0.98$ (blue curve) and $q = 0.9$ (red curve)

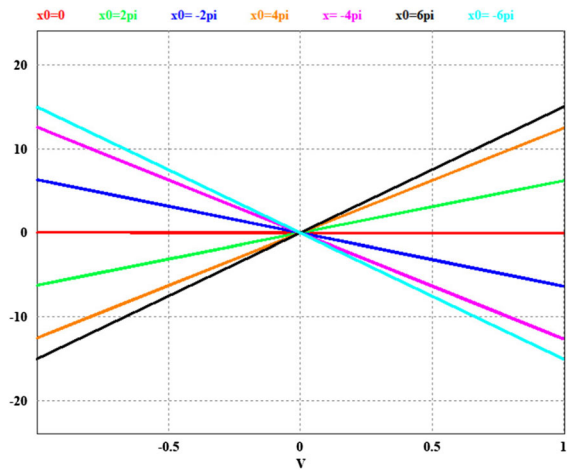

Fig. 20 Coexisting pinched hysteresis loops obtained from the memristor circuit in PSIM simulation under different initial capacitor voltages $\pm 6\pi$ V, $\pm 4\pi$ V, $\pm 2\pi$ V, 0V

5 Conclusion

In this paper, a fractional-order multistable locally active memristor is proposed for the first time, which has infinitely many coexisting pinched hysteresis loops under different initial states and wide locally active

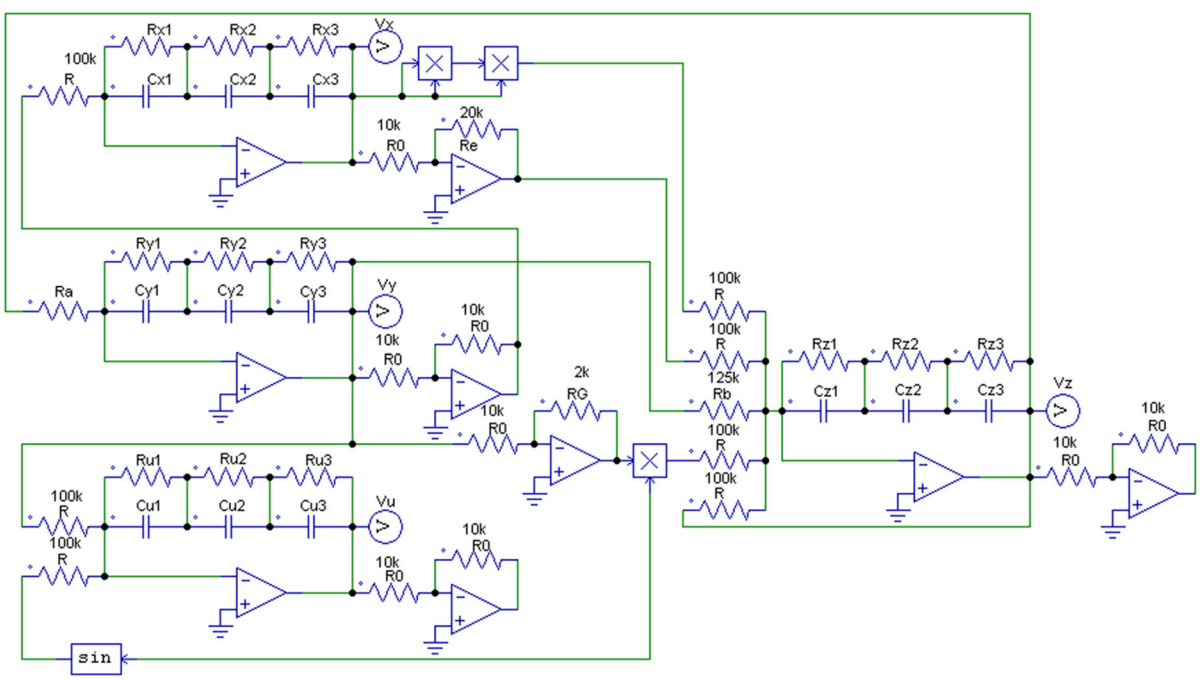

Fig. 21 Circuit configuration of the fractional-order multistable locally active memristive chaotic system

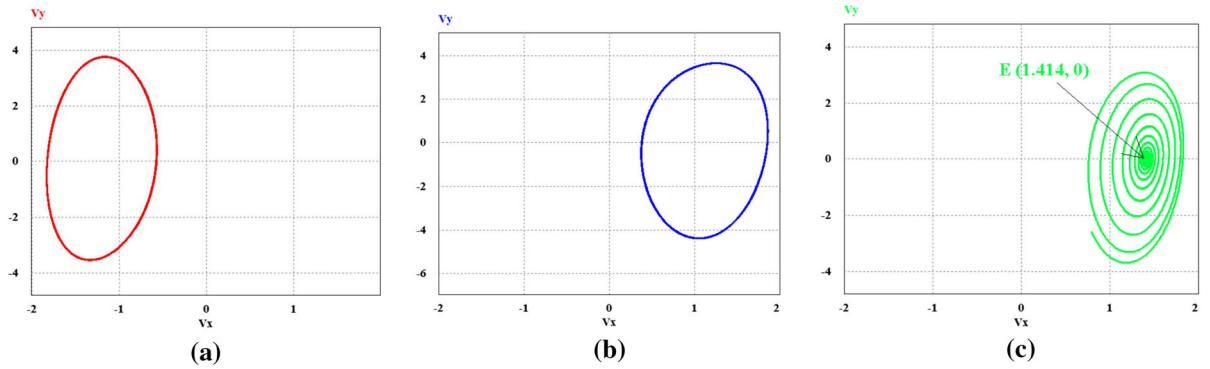

Fig. 22 Coexisting attractors obtained from the fractional-order chaotic system circuit in PSIM simulation for different initial values and $q = 0.9$. **a** Initial values (0.1V, −0.1V, −0.1V, −0.1V). **b** Initial values (0.1V, 0.1V, −0.1V, 0V). **c** Initial values (0.1V, 0.1V, −0.1V, −7V)

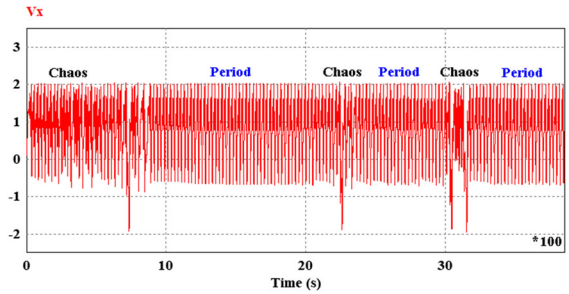

Fig. 23 The behavior of transient transition obtained from the fractional-order chaotic system circuit in PSIM simulation

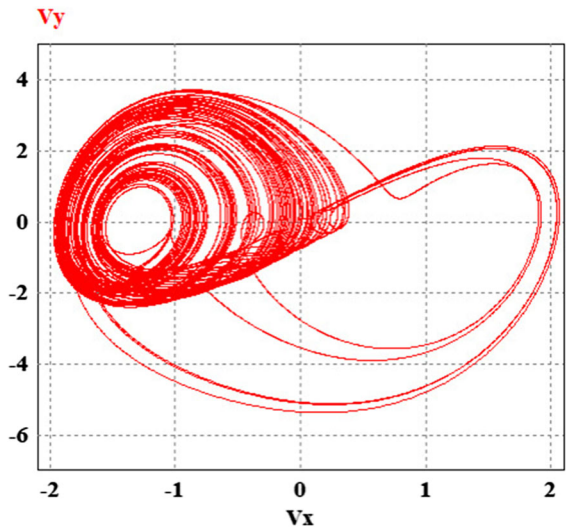

Fig. 24 The behavior of state jump obtained from the fractional-order chaotic system circuit in PSIM simulation when $q = 0.97$

regions. It is found that this fractional-order memristor has stronger locally active and memory characteristics and larger nonvolatile ranges than integer-order memristor. The fractional-order chaotic system based on the fractional-order multistable locally active memristor is explored. The stability of equilibrium points and the effect of α-order on equilibrium points are analyzed. It is found that oscillations occur only within the locally active region. By bifurcation analysis and Lyapunov exponent spectrum analysis, it is found that the system has extremely rich dynamics such as infinitely many discrete equilibrium points, multistability and anti-monotonicity. Interestingly, the system presents two phenomena that have not been found in other chaotic systems, which are state jump and transient transition. Finally, the circuit simulation of the fractional-order multistable locally active memristive chaotic system using PSIM is carried out to verify the validity of the numerical simulation results.

Acknowledgements This work is supported by the Major Research Plan of the National Natural Science Foundation of China (No.91964108), the National Natural Science Foundation of China (No.61971185) and Natural Science Foundation of Hunan Province (2020JJ4218)

Declarations

Conflict of interest The authors declare that they have no conflicts of interest.

References

1. Petráš, I.: A note on the fractional-order Chua's system. Chaos, Solitons Fractals **38**(1), 140–147 (2008)
2. Ma, J., Tang, J.: A review for dynamics in neuron and neuronal network. Nonlinear Dyn. **89**(3), 1569–1578 (2017)
3. Bao, H., Liu, W., Ma, J., Wu, H.: Memristor initial-Offset boosting in memristive HR neuron model with hidden firing patterns. Int. J. Bifurc. Chaos **30**(10), 2030029 (2020)
4. Zhou, P., Yao, Z., Ma, J., Zhu, Z.: A piezoelectric sensing neuron and resonance synchronization between auditory neurons under stimulus. Chaos, Solitons Fractals **145**, 110751 (2021)
5. Li, Z., Zhou, H., Wang, M., et al.: Coexisting firing patterns and phase synchronization in locally active memristor coupled neurons with HR and FN models. Nonlinear Dyn. (2021). https://doi.org/10.1007/s11071-021-06315-4
6. Yao, W., Wang, C., Sun, Y., Zhou, C., Lin, H.: Exponential multistability of memristive Cohen–Grossberg neural networks with stochastic parameter perturbations. Appl. Math. Comput. **386**, 125483 (2020)
7. Lin, H., Wang, C., Yao, W., Tan, Y.: Chaotic dynamics in a neural network with different types of external stimuli. Commun. Nonlinear Sci. Numer. Simul. **90**, 105390 (2020)
8. Lin, H., Wang, C., Tan, Y.: Hidden extreme multistability with hyperchaos and transient chaos in a Hopfield neural network affected by electromagnetic radiation. Nonlinear Dyn. **90**(3), 2369–2386 (2020)
9. Deng, Q., Wang, C., Yang, L.: Four-wing hidden attractors with one stable equilibrium point. Int. J. Bifurc. Chaos **30**(06), 2050086 (2020)
10. Yu, F., Qian, S., Chen, X., et al.: Chaos-based engineering applications with a 6D memristive multistable hyperchaotic system and a 2D SF-SIMM hyperchaotic map. Complexity **2021**, 6683284 (2021)
11. Wang, C., Xia, H., Zhou, L.: A memristive hyperchaotic multiscroll jerk system with controllable scroll numbers. Int. J. Bifurc. Chaos **27**(06), 1750091 (2017)
12. Wu, R., Wang, C.: A new simple chaotic circuit based on memristor. Int. J. Bifurc. Chaos **26**(09), 1650145 (2016)
13. Cheng, G., Wang, C., Xu, C.: A novel hyper-chaotic image encryption scheme based on quantum genetic algorithm and compressive sensing. Multimed. Tools Appl. **79**(39), 29243–29263 (2020)
14. Deng, J., Zhou, M., Wang, C., Wang, S., Xu, C.: Image segmentation encryption algorithm with chaotic sequence generation participated by cipher and multi-feedback loops. Multimed. Tools Appl. (2021). https://doi.org/10.1007/s11042-020-10429-z
15. Zeng, J., Wang, C.: A novel hyperchaotic image encryption system based on particle swarm optimization algorithm and cellular automata. Secur. Commun. Netw. **2021**, 6675565 (2021)
16. Chen, X., Qian, S., Yu, F., et al.: Pseudorandom number generator based on three kinds of four-wing memristive hyperchaotic system and its application in image encryption. Complexity **2020**, 8274685 (2020)
17. Xu, C., Sun, J., Wang, C.: An image encryption algorithm based on random walk and hyperchaotic systems. Int. J. Bifurc. Chaos **30**(4), 2050060 (2020)
18. Hong, Q., Yan, R., Wang, C., Sun, J.: Memristive circuit implementation of biological nonassociative learning mechanism and its applications. IEEE Trans. Biomed. Circuits Syst. **14**(5), 1036–1050 (2020)
19. Hong, Q., Shi, Z., Sun, J., Du, S.: Memristive self-learning logic circuit with application to encoder and decoder. Neural Comput. Appl. (2020). https://doi.org/10.1007/s00521-020-05281-z
20. Coopmans, C., Petráš, I., Chen, Y.: Analogue fractional-order generalized memristive devices. In: Proceedings of the ASME 2009 International Design Engineering Technical Conferences and Computers and Information in Engineering Conference, San Diego, USA (2009)
21. Petráš, I.: Fractional-order memristor-based Chua's circuit. IEEE Trans. Circuits. Syst. II Exp. Briefs **57**(12), 975–979 (2010)
22. Cafagna, D., Grassi, G.: On the simplest fractional-order memristor-based chaotic system. Nonlinear Dyn. **70**(2), 1185–1197 (2012)
23. Teng, L., Iu, H.H., Wang, X., Wang, X.: Chaotic behavior in fractional-order memristor-based simplest chaotic circuit using fourth degree polynomial. Nonlinear Dyn. **77**(1), 231–241 (2014)
24. Si, G., Diao, L., Zhu, J.: Fractional-order charge-controlled memristor: theoretical analysis and simulation. Nonlinear Dyn. **87**(4), 2625–2634 (2017)
25. Yang, N., Xu, C., Wu, C., et al.: Fractional-order cubic nonlinear flux-controlled memristor: theoretical analysis, numerical calculation and circuit simulation. Nonlinear Dyn. **97**(1), 33–44 (2019)
26. Yu, Y., Wang, Z.: A fractional-order memristor model and the fingerprint of the simple series circuits including a fractional-order memristor. Acta Physica Sinica **64**(23), 238401 (2015)
27. Yu, Y., Wang, Z.: Initial state dependent nonsmooth bifurcations in a fractional-order memristive circuit. Int. J. Bifurc. Chaos **28**(07), 1850091 (2018)
28. Chua, L.: If it's pinched it's a memristor. Semicond. Sci. Technol. **29**(10), 104001 (2014)
29. Chua, L.: Local activity is the origin of complexity. Int. J. Bifurc. Chaos **15**(11), 3435–3456 (2005)
30. Corinto, F., Ascoli, A., Gilli, M.: Nonlinear dynamics of memristor oscillators. IEEE Trans. Circuits Syst. I Reg. Pap. **58**(6), 1323–1336 (2011)
31. Gibson, G.A., Musunuru, S., Zhang, J., et al.: An accurate locally active memristor model for S-type negative differential resistance in NbOx. Phys. Lett. A **108**(2), 023505 (2016)
32. Weiher, M., Herzig, M., Tetzlaff, R., et al.: Pattern formation with locally active S-type NbOx memristors. IEEE Trans. Circuits Syst. I Reg. Pap. **66**(7), 2627–2638 (2019)
33. Chua, L.: Everything you wish to know about memristors but are afraid to ask. Radioengineering **24**(2), 319–368 (2015)
34. Mannan, Z.I., Choi, H., Kim, H.: Chua corsage memristor oscillator via hopf bifurcation. Int. J. Bifurc. Chaos **26**(04), 1630009 (2016)
35. Jin, P., Wang, G., Iu, H.H., Fernando, T.: A locally active memristor and its application in a chaotic circuit. IEEE Trans. Circuits Syst. II Exp. Briefs **65**(2), 246–250 (2017)
36. Chang, H., Wang, Z., Li, Y., Chen, G.: Dynamic analysis of a bistable bi-local active memristor and its associated oscillator system. Int. J. Bifurc. Chaos **28**(08), 1850105 (2018)

37. Mannan, Z.I., Yang, C., Kim, H.: Oscillation with 4-lobe Chua corsage memristor. IEEE Circuits Syst. Mag. **18**(2), 14–27 (2018)
38. Dong, Y., Wang, G., Chen, G., et al.: A bistable nonvolatile locally-active memristor and its complex dynamics. Commun. Nonlinear Sci. Numer. Simul. **84**, 105203 (2020)
39. Tan, Y., Wang, C.: A simple locally active memristor and its application in HR neurons. Chaos **30**(5), 053118 (2020)
40. Lin, H., Wang, C., Sun, Y., Yao, W.: Firing multistability in a locally active memristive neuron model. Nonlinear Dyn. **100**(4), 3667–3683 (2020)
41. Zhu, M., Wang, C., Deng, Q., Hong, Q.: Locally active memristor with three coexisting pinched hysteresis loops and its emulator circuit. Int. J. Bifurc. Chaos **30**(13), 2050184 (2020)
42. Lin, H., Wang, C., Hong, Q., Sun, Y.: A multi-stable memristor and its application in a neural network. IEEE Trans. Circuits Syst. II Exp. Briefs **67**(12), 3472–3476 (2020)
43. Gorenflo, R., Mainardi, F.: Fractional Calculus. Fractals and Fractional Calculus in Continuum Mechanics. Springer, Vienna (1997)
44. Podlubny, I.: Fractional Differential Equations. Academic Press, San Diego (1999)
45. Kengne, J., Njitacke, Z.T., Fotsin, H.: Dynamical analysis of a simple autonomous jerk system with multiple attractors. Nonlinear Dyn. **83**(1), 751–765 (2016)
46. Ahmed, E., El-Sayed, A., El-Saka, H.: Equilibrium points, stability and numerical solutions of fractional-order predator-prey and rabies models. J. Math. Anal. Appl. **325**(1), 542–553 (2007)
47. El-Saka, H., Ahmed, E., Shehata, M., El-Sayed, A.: On stability, persistence, and Hopf bifurcation in fractional order dynamical systems. Nonlinear Dyn. **56**(1), 121–126 (2009)
48. Tavazoei, M., Haeri, M.: A proof for non existence of periodic solutions in time invariant fractional order systems. Automatica **45**(8), 1886–1890 (2009)
49. Kaslik, E., Sivasundaram, S.: Non-existence of periodic solutions in fractional-order dynamical systems and a remarkable difference between integer and fractional-order derivatives of periodic functions. Nonlinear Anal. Real World Appl. **13**(3), 1489–1497 (2012)
50. Danca, M.-F., Fečkan, M., Kuznetsov, N.V., Chen, G.: Complex dynamics, hidden attractors and continuous approximation of a fractional-order hyperchaotic PWC system. Nonlinear Dyn. **91**(4), 2523–2540 (2018)
51. Danca, M.-F., Fečkan, M., Chen, G.: Impulsive stabilization of chaos in fractional-order systems. Nonlinear Dyn. **89**(3), 1889–1903 (2017)
52. Kang, Y.-M., Xie, Y., Lu, J.-C., Jiang, J.: On the nonexistence of non-constant exact periodic solutions in a class of the Caputo fractional-order dynamical systems. Nonlinear Dyn. **82**(3), 1259–1267 (2015)
53. Danca, M.-F., Kuznetsov, N.V.: Matlab code for Lyapunov exponents of fractional-order systems. Int. J. Bifurc. Chaos **28**(5), 1850067 (2018)
54. Diethelm, K., Ford, N.J., Freed, A.D.: A predictor-corrector approach for the numerical solution of fractional differential equations. Nonlinear Dyn. **29**, 3–22 (2002)
55. Li, C., Sprott, J.C.: Multistability in the Lorenz system:a broken butterfly. Int. J. Bifurc. Chaos **24**(10), 1450131 (2014)
56. Yu, Y., Bao, H., Shi, M., et al.: Complex dynamical behaviors of a fractional-order system based on a locally active memristor. Complexity **2019**, 2051053 (2019)
57. Wu, J., Wang, G., Iu, H.H., et al.: A nonvolatile fractional order memristor model and its complex dynamics. Entropy **21**(10), 955 (2019)
58. Pham, V.T., Kingni, S.T., et al.: A simple three-dimensional fractional-order chaotic system without equilibrium: Dynamics, circuitry implementation, chaos control and synchronization. AEU Int. J. Electron. Commun. **78**, 220–227 (2017)
59. Min, F., Shao, S., Huang, W., Wang, E.: Circuit implementations, bifurcations and chaos of a novel fractional-order dynamical system. Chin. Phys. Lett. **32**(3), 030503 (2015)